An Experimental Investigation on the Characteristics of Heat Pipes with Annular Type Composite Wick Structure

Joseph Seo¹, Daegeun Kim¹, Hansol Kim², Yassin A. Hassan^{1,2}

¹Department of Nuclear Engineering, Texas A&M University, 3133 TAMU, College Station, Texas

²J. Mike Walker '66 Department of Mechanical Engineering, Texas A&M University, College Station, Texas seojoseph@tamu.edu

Abstract

An experimental investigation has been conducted on the hydraulic characteristics of annular type wick structures for heat pipes. An experimental facility which can measure porosity, permeability, and effective pore radius of the wick structures in a vacuum condition is established. Nine different types of multi-layered (6 layers in total) composite screen meshes are characterized. Based on the measurement results, a wick structure composed of one layer of 100×100 mesh, three layers of 400×400 mesh, and two layers of 60×60 mesh is determined to have the highest permeability to effective pore radius ratio (K/r_{eff}) and was selected as a targeted sample. The wick-to-wall gap effect on the hydraulic characteristics of annular type wick structure is also investigated by measuring the permeability and effective pore radius of the sample wick structure with varying gap widths. The result shows that the permeability increases as the gap increases from 0 mm to 1.2 mm. After a peak at 1.2 mm, the permeability decreases as the gap increases and converges to the value of the case measured without a wall structure. The effective pore radius becomes smaller as the gap increases, making a peak at a gap distance of 1.2 mm. This result implies that there is an optimal point in gap distance which is determined to be 1.2 mm for the selected composite mesh structure. A capillary limitation correlation with a multiplying factor which explains the enhanced performance of the wick due to the gap is suggested. An annular wick type heat pipe is constructed and tested. The capillary limitation of the heat pipe showed good agreement with the suggested correlation.

1. Introduction

A heat pipe is a passive heat transfer device with high thermal conductance that utilizes both the thermal conduction of the solid enclosure and the phase change of the internal working fluid [1]. The working fluid passively circulates inside of the heat pipe and transfers heat from the evaporator region to the condenser region by the principle of the convective heat transfer with the phase change phenomena. Due to its high conductance and passive working characteristics, great efforts have been made to apply heat pipes to various industries since its first suggestion by Gaugler [2] and independent invention by Grover [3]. In the early days, heat pipes were actively studied for use in space [4]. With the recent rise of the electronics industry, the application of small sized heat pipes as cooling components in high heat-density systems has been intensively studied [5]. Meanwhile, the use of a heat pipes as a heat transfer device for a large-scale system has been actively discussed, such as utilization of heat pipe system to increase the efficiency of solar cells [6]. In the nuclear industry, heat pipes have also been proposed as a passive cooling system of nuclear power plants in a station black out (SBO) scenario due to beyond design-basis accidents (BDBA) [7,8]. In addition, research is being conducted on liquid metal heat pipes with annular wick structures that can be used in micro nuclear reactors [9]. The surrounding air, lakes, and seas could all act as heat sinks for the earth's micro reactor. However, due to insufficient atmosphere on the Moon and Mars, radiation is the only viable option for space missions which emphasizes the need of heat pipe application to the reactor. As a result, liquid metal heat pipes with various working fluid and operating temperature have been suggested and studied by multiple research groups. The operating temperature range of Kilopower and SAIRS heat pipes using Na as the working fluid is 1050K-1200K [10-12], while HOMER15/25 and eVinci heat pipes using Na/K is 880K-920K [13,14]. The MSR-A and HP-STMCs use Li as the working fluid and operate between 1500 and 1800K [11,15], whereas the MSR-B uses K and operates between 930 and 1500K [16].

The classification of heat pipes can be achieved by considering the source of force used to return the condensed fluid from the condenser region to the evaporator region. For example, a wickless heat pipe, also called as a thermosyphon, uses gravity to transfer liquid to the evaporator. A heat pipe with wick, which is the most common type, uses capillary force generated by porous media as the source of liquid transport. This type of heat pipe can be used irrespective of the direction of heat transfer to gravity, which is a huge advantage in its range of applications. Since the primary heat transport medium is liquid, characteristics of the wick structure dominates overall performance of the heat pipe.

Based on the theories of porous media, the wick structure can be characterized with parameters such as porosity (\mathcal{E}), pore radius ($\mathit{r}_{e\!f\!f}$), and permeability (K) [17]. Porosity is a volume fraction of the voids inside porous media over the total volume. Pore radius, or pore size, is an average size of voids inside the porous media. This parameter is directly related to the capillary pressure from the Young-Laplace equation. This parameter should be small enough to acquire a large capillary pressure difference between the evaporator and condenser region. Permeability, on the other hand, represents ability of fluids to flow through the porous media. For a heat pipe, the permeability is a parameter of the wick resistance to liquid which flows in the axial direction of the pipe. It needs to be large to obtain a small liquid pressure drop along the wick structure [18]. In addition to these hydraulic parameters of wick structures, the thermal conductivity is also an important thermal characteristic to determine the performance of the heat pipe.

From the previous description, it can be inferred that wick structures inside heat pipes should have a small pore radius and a high permeability. However, having a low pore radius and a high permeability is hard to achieve in most wick designs [18]. In other words, the two parameters become competing factors to each other in a homogeneous wick. A homogeneous wick with a small pore radius might have high capillary pressure but it also has a small permeability which will create a high resistance to the liquid flow. There can be two ways to overcome this problem. First, a composite wick structure, which is composed of various sizes of pores can be used. The composite wick structures provide high capillary pressure by having small pores, while employing high permeability from large pores. The simplest composite wick can be constructed by wrapping multiple layers of screen mesh with different pore sizes, which is a multi-layered composite mesh screen wick [18]. The other way to overcome the tradeoff problem of the pore size and the permeability is to introduce an extra flow path for liquids other than wick structures. A heat pipe with an annular type wick structure, for example, has a gap space between the tube and the wick structure. Since condensed fluid can travel through the gap, the heat pipe with an annular wick has a significantly lower pressure drop when it is compared to the heat pipe with homogeneous wick [19]. The advantage of introducing the gap can be more clearly emphasized when the pressure drop values for the gap and porous media are quantitively compared. Assuming a laminar flow through 1m of channel, water experiences approximately 6 times smaller pressure drop when it travels through the 0.7 mm gap instead of a porous media with 10⁻¹¹ m² of permeability from the calculation using Darcy's law.

Recently, the implementation of the annular composite wick heat pipe as a principal heat transmission system of the micro reactor is being carefully examined due to its merits indicated above. Failure of a heat pipe can result in serious contamination issues, such as the release of working fluid. Because the heat pipe is a passive device, the user cannot change the operation characteristics of the heat pipe after installation. As a result, for the reactor's safety and durability, the performance of the heat pipe under various conditions should be investigated. Pauluis and Lang used a theoretical approach to analyze the pressure drop in the wick structure of annular wick heat pipes using hydrogen, nitrogen, and oxygen as working fluids [19]. The

steady-state cyclic performance of a sodium heat pipe reactor was investigated by Paripatyadar and Richardson using a daily solar cycle in the 600–900 C range [20]. Richardson et al. simulated and tested a sodium heat pipe reactor, obtaining data such as axial and radial temperature profiles, energy flux transformation, and flux profiles for each temperature range [21]. Rosenfeld et al. reported on the operating lifetime and reliability of sodium heat pipes with different wall materials [22]. Gotoh and Hill investigated the stability and reproducibility of sodium heat pipes [23]. Reid et al. measured the heat rejection rate in the operating temperature range of 13 sodium heat pipes using the SAFE-30 core configuration [24].

However, there are only a limited number of studies on heat pipe design and modeling. To the author's best knowledge, there is huge lack of experimental data and models that can support the design of the annular type composite wick heat pipe. To be specific, important design parameters that might seriously affect the performance of the heat pipe such as composition of the wick structure and gap distance have not yet been studied even though the importance of these parameters becomes more apparent. The importance of the research increases when the predictions of the heat transfer performance and the operating limitations are directly related to the safety of the system. In the application of the heat pipe into a high temperature micro nuclear reactor, for instance, experimental investigation of the design parameters and models are necessary to determine heat pipe performance in continuous operation as well as the safety margins of the system, which is the primary motivation of this study.

In this study, therefore, the characteristics of the annular type composite wick stricture are intensively studied. A total of nine combinations of the multi-layered screen meshes are constructed and their performances are tested. Also, the effect of the wall to the performance of the wick structures is investigated. Different gap distances between wall and wick structure are used to address the investigation. The performance of wick structures is characterized using K/r_{eff} values. The results obtained from wick characterization experiment is expanded to the heat pipe performance experiment. The capillary limitation of the heat pipe is determined and a model that can include understandings of the wick characterization is suggested. The work will increase insight into understanding heat pipes with annular type composite wick structures. Also, the data and model provided in this study might help to build a heat pipe with optimized performance in a targeted condition.

2. Experimental Method

The experimental component of this study is divided into two components. The first study examines the characteristics of the composite wick structures with varying wick compositions. Measurements for porosity were made, followed by an experimental procedure to determine the permeability and effective pore radius. This ratio, K / r_{eff} , is an important indicator for heat pipe performance. The effect on K / r_{eff} due to the gap distance between the wick structure and the wall is also investigated. As mentioned in the previous section, resistance of the flow for the annular wick type heat pipe appears as a combination of Darcy flow in the porous media and laminar flow in the annulus. In this case, K / r_{eff} of wick and wall assembly can usefully explain the combined resistance and used as an indicator of the heat pipe performance in terms of capillary limitation.

Results obtained from the wick characterization experiment are then expanded to a heat pipe performance experiment. A heat pipe is constructed with the mesh composition determined to have the highest K / r_{eff} value. After operating this heat pipe at a range of temperatures and power levels, the capillary limitation of the heat pipe is determined and a model reflecting the wick characterization is presented. This work will

provide valuable insights into heat pipes with annular type composite wick structures. The data and model produced by this study will help to design heat pipes with optimized performance under required conditions.

2.1. Wick Characterization Experiment

2.1.1. Wick Structure Construction

In this experiment, 9 wick variations, each with 6 mesh screen layers, were constructed using three types of mesh: 60 by 60, 100 by 100, and 400 by 400. Detailed information of the 9 samples is shown in Table 1. Because wick structures are constructed manually in this study, there will be uncertainties caused by the manufacturing process. The uncertainties are quantified by replicating the construction of each of the 9 cases 12 times. The porosity of 12 meshes are measured by the method introduced in the next section, and the deviation of the measurement are determined to quantify the uncertainty. The results showed that the measured porosities of 12 meshes have a standard deviation of $\pm 0.81\%$ in a comparison with the averaged value.

Table 1. Composition of the multi-layered composite screen wicks

	Total	Mesh composition					
Case #	number of layers	100-mesh (inside layer)	400-mesh (middle layer)	60-mesh (outside layer)			
1		6	0	0			
2		0	6	0			
3		0	0	6			
4		2	2	2			
5	6	1	3	2			
6		2	3	1			
7		2	1	3			
8		3	2	1			
9		3	3	2			

To build the wick sample, each mesh screen was cut to be 25.4 mm by 101.6 mm. Six mesh screens were stacked on top of each other in the order shown in Table 1. The edges of the stacked meshes were then spotwelded create a bond between adjacent meshes. The constructed mesh structures were thoroughly washed using 70 % isopropyl alcohol as a final step. Figure 1 shows the configuration of the wick assembly for the wall effect experiment. It is composed of a wall with a clamp at the top, the wick, and the shim structures. Shim structures were inserted between the wall and the wick in the clamped section of the assembly to creating a controlled the gap distance ranging from 0 mm to 20 mm.

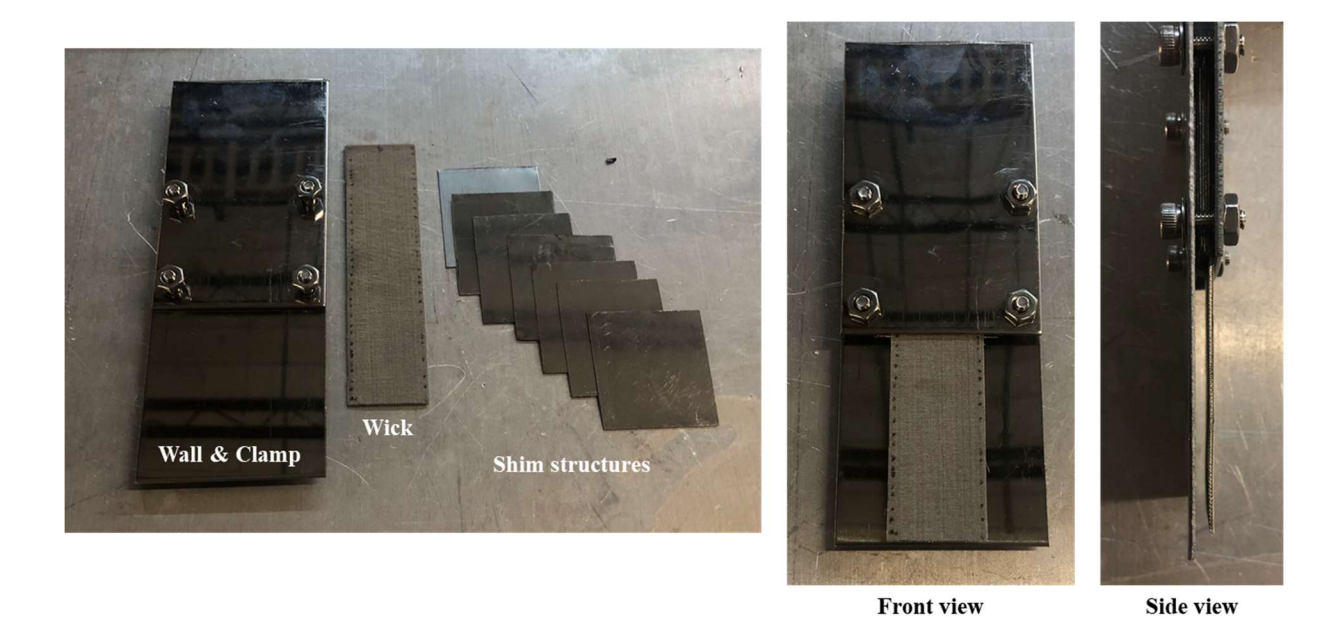


Figure 1. The configuration of the wick assembly for the wall effect experiment.

2.1.2. Porosity Measurement

Porosity is a ratio of the void volume in a porous media over the total volume. In this study, mass and density data are used to measure porosities of different wick structures. Considering time required for wetting and drying, ethanol is used as a wetting fluid. A bench-top digital scale with ± 0.001 g of resolution (or readability) is prepared to measure the mass of the dry and wet mesh. The void volume of a mesh can be obtained from the ethanol mass required to fully wet (or saturate) the mesh. First, the mass of dried mesh (m_{mesh}), is measured using the scale. Then, the mesh was fully immersed in ethanol for a duration of about 10 seconds before being weighed again. By subtracting the mass of dried mesh from the saturated mesh, the amount of liquid inside of the mesh (m_{liquid}) is determined. The porosity is calculated using the known density of the ethanol and mesh using Eq.1.

$$\frac{1}{\varepsilon} = 1 + \frac{m_{mesh} \rho_{liquid}}{m_{liquid} \rho_{mesh}}$$
 Eq.1

Uncertainty is introduced into this procedure by to both the scale and liquid loss due to evaporation, a difficult value to quantify. Thus, the same procedure is repeated 10 times to obtain the averaged mass data. The result showed a standard deviation of $\pm 0.30\%$.

2.1.3. Permeability and Effective Pore Radius Measurement

To measure permeability and effective pore radius of each wick sample, the method suggested by Holley and Faghri (2004)[25] was used. In this method, a transcendental equation based on mesh geometry, fluid properties, and the height of a rising liquid at a given time is derived using the pressure balance for the rise of liquid in a vertical wick. Because the exact location of a liquid front can be difficult to determine in the

case of non-homogeneous wick structure, the height is substituted with the mass of the rising liquid. This produces the following equation:

$$t_{Holley\&Faghri} = f(K, r_{eff}, m_{exp}) = -\frac{\varepsilon \mu_l}{\rho_l^2 g^2 K} \left[\frac{2\sigma}{r_{eff}} \ln \left(1 - \frac{gr_{eff}}{2\sigma A_{wick} \varepsilon} m_{exp} \right) + \frac{g}{A_{wick} \varepsilon} m_{exp} \right]$$
 Eq.2

Here, σ is the surface tension of the working fluid, A_{wick} is the cross-sectional area of the wick, μ_l represents the viscosity of the working fluid, ρ_l is the density of the working fluid, and g is the gravitational acceleration. When the liquid properties and geometric parameters are known, the time variable, $t_{Holley\&Faghri}$, can be calculated from three unknowns, permeability (K), effective pore radius(r_{eff}), and mass of the liquid (m_{exp}) pulled up by the mesh. By introducing a variable for experiment time, (t_{exp}), as shown in Eq. 3, and performing a vertical liquid rising experiment using a sintered mesh sample, Holley and Faghri obtained several pairs of mass (m_{exp}) and time (t_{exp}) data. Then, to find the solution, a sample space of permeability and effective pore radius was set, and the result of the mean absolute percent deviation of time values (t_{exp}) of the data set from calculated time ($t_{Holley\&Faghri}$) was plotted in space. The true values for permeability and effective pore radius were then determined to be where the error between t_{exp} and $t_{Holley\&Faghri}$ was smallest.

$$t_{\exp} - t_{Holley\&Faghri} = f(K, r_{eff}, m_{\exp}, t_{\exp}) = t_{\exp} + \frac{\varepsilon \mu_{l}}{\rho_{l}^{2} g^{2} K} \left[\frac{2\sigma}{r_{eff}} \ln \left(1 - \frac{gr_{eff}}{2\sigma A_{wick} \varepsilon} m_{\exp} \right) + \frac{g}{A_{wick} \varepsilon} m_{\exp} \right] = 0$$

$$\begin{cases} t_{\exp} = \left(t_{1}, t_{2}, t_{3}, \dots, t_{n} \right), \\ m_{\exp} = \left(m_{t=t_{1}}, m_{t=t_{2}}, m_{t=t_{3}}, \dots, m_{t=t_{n}} \right) \end{cases}$$
Eq. 3

The approach introduced above is adopted in this study. Figure 2 shows the experimental setup for measuring the permeability and effective pore radius of the wick structures. An acrylic vacuum chamber was prepared and connected to a vacuum pump to obtain a vacuum condition inside. A vacuum pump with 1.5×10^{-2} torr of maximum vacuum pressure and 4.72 liter per second (LPS) of max flow rate was used in this study. The vacuum pressure was monitored by an analog pressure gauge connected between vacuum chamber and the pump. A rod of 3.18 mm in diameter was installed through the top of the chamber using an O-ring compression fitting. The fitting allows the rod to move up and down while maintaining the vacuum condition in the chamber. The dried wick structure (or the wall and mesh assembly in the case of the wall effect experiment) was placed in the chamber held by a clamp at the end of the rod. A bench-top digital scale with ± 0.001 g of resolution (or readability) was located at the bottom of the vacuum chamber. The repeatability (or standard deviation) of the scale was ± 0.002 g. A petri dish filled with 99.9% pure ethanol was placed on the scale and used to measure the rising speed of the fluid.

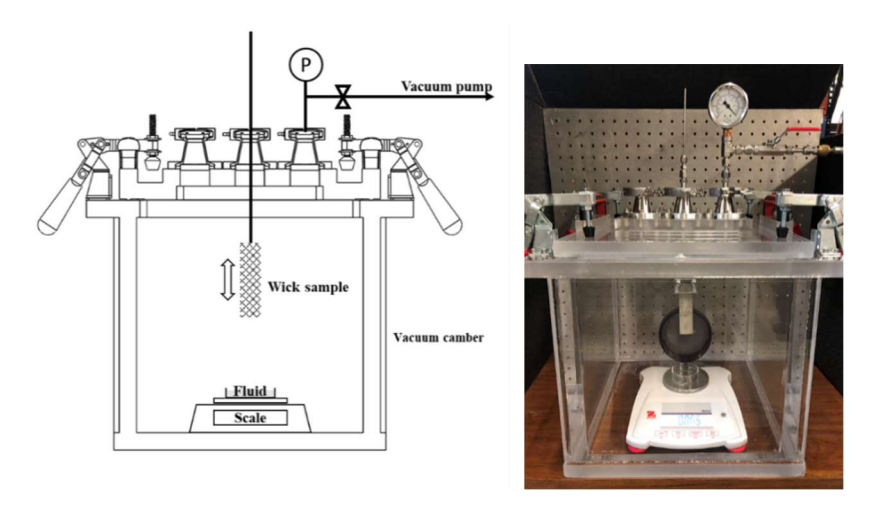


Figure 2. The schematic (left) and picture (right) of the wick characterization experimental setup

The experiment begins by filling the petri dish with ethanol up to a specified level and taring the scale. The wick is fixed, and the vacuum flange (top cover of the vacuum chamber) is attached to the chamber. The chamber is vacuumed down to -90 kPa of vacuum pressure using the vacuum pump. Then, the wick is slowly lowed toward the petri dish. When the wick reaches the fluid and its tip is submerged into ethanol, the wick is stopped, and its height is maintained. The reading of the scale is recorded using a camera with 30 fps of capturing frequency. After the wick is determined to be saturated by checking the change of mass, the valve of the chamber is opened to recover the pressure and the wick is removed from the chamber.

In Figure 3, the mass retained by the composite mesh case number 8 in the Table 1 is shown as an example. It can be noticed that the rate of mass decreases during the measured time and becomes saturated after several minutes. From the data, five pairs of time and mass are selected. In this study, 0.667, 1.67, 3.33, 5.00, and 6.67 s of time and the mass at those time values are used to calculate the permeability and effective pore radius of the wicks.

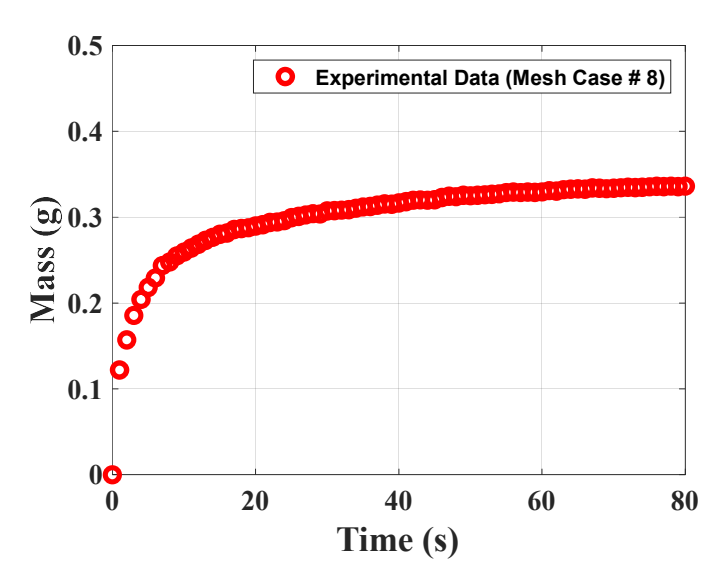


Figure 3. The example of the mass retained by the composite mesh (Case #8)

2.2. Heat Pipe Experiment

2.2.1. Heat Pipe Construction

In this study, an annular type multi-layered rolled composite screen mesh made of stainless steel is used as a wick structure of the heat pipe. The cross-sectional imaging of the heat pipe, shown in Figure 5, was done using a traditional camera and by a micro-CT scan. The wick structure is composed of 6 layers of screen mesh. From the inside of the heat pipe, one layer of a 100-mesh screen, three layers of 400-mesh screens, and two layers of 60-mesh screens were rolled to compose the wick structure. As will be shown, this design decision was informed by the mesh composition determined to have the most favorable performance characteristics determined by the results of the wick characterization experiment. To fabricate the wick structure, mesh screens were wrapped around a 1.2 m long rod with a diameter of 17.46 cm (11/16 inches). The cylindrical shape of the wick structure was retained by spot welds along the axial direction with 1.5 \sim 2.0 mm intervals. After removing the rod, the wick structure was inserted into a 1.2 m 304 L seamless stainless-steel pipe with an outer and inner diameter of 25.4 mm and 22.1 mm, respectfully. The dimensions of the manufactured wick are 18.1 mm of inner diameter, 1.12 mm of thickness, and 20.3 mm of outer diameter, which leaves 0.95 mm of gap between the inner surface of the stainless tube when inserted. The gap between the wick structure and inner wall of the tube was maintained by wire wrapping each end of wick structure.

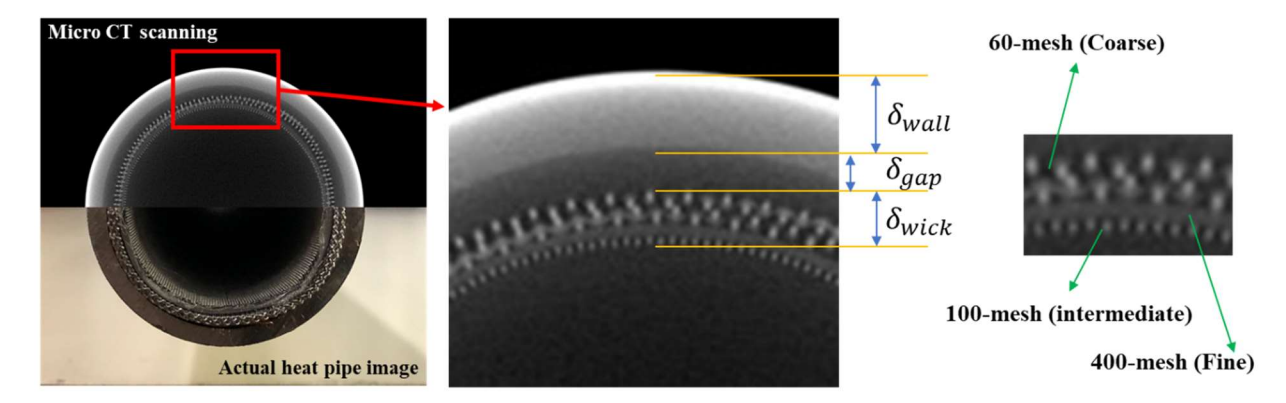


Figure 4. The cross-sectional design of the wick structure inside the heat pipe taken by micro-CT scanning

Heat pipe fabrication consists of cleaning, vacuuming, fluid filling, and sealing processes. The inside of the stainless-steel pipe and wick structure was cleaned using ethanol. Each end of the pipe was closed using compression fittings. One side of the pipe was connected to the vacuum pump and working fluid insertion system. After -90 kPa of vacuum pressure was achieved by the vacuum pump, 160 mL of DI water was inserted into the pipe as a working fluid. Then, the pipe was sealed by a locking ball valve connected to the vacuum pump. As a final step of the fabrication, leakage was checked to verify the condition inside of the heat pipe.

2.2.2. Heat Pipe Performance Experimental Facility

Figure 5 shows the schematic and a picture of the heat pipe experimental setup. The experimental setup consists of three parts, the heat pipe, the heating & cooling regions, and the measurement system. The 1.2

m stainless steel heat pipe with an annular multi-layered composite screen mesh was fixed with a horizontal geometry. The length ratio of the evaporating, adiabatic, and condensing region was set as 1:1:1. A heating coil with 468 W of maximum power was wrapped on the evaporator section of the heat pipe. The heater was connected to a transformer and power meter to control the power output. A water jacket with a variable flow rate was installed at the condensing region of the heat pipe to remove the heat transferred by the heat pipe. The inlet temperature of the cooling fluid inside the water jacket was controlled by a Merilin M33 chiller from the Neslab company. The inlet and outlet temperatures were measured using K-type thermocouples and the flow rate was measured using a flow meter to monitor the energy balance of the heat pipe module. Evaporating and adiabatic regions of the heat pipe were insulated using glass wool with a thickness of 50 mm.

The temperature distribution along the outer surface of the heat pipe was measured using K-type thermocouples. Three thermocouples were attached at the outer surface of the evaporator region, and one thermocouple was fixed at the middle of the adiabatic region. Two thermocouples were inserted into the water jacket and their end points were fastened at the outer surface for the heat pipe. To monitor the inner pressure, four analog pressure gauges were used. Four pressure gauges, one at the evaporator region, two at the adiabatic region, and one at the end of the condenser region, were installed along the heat pipe.

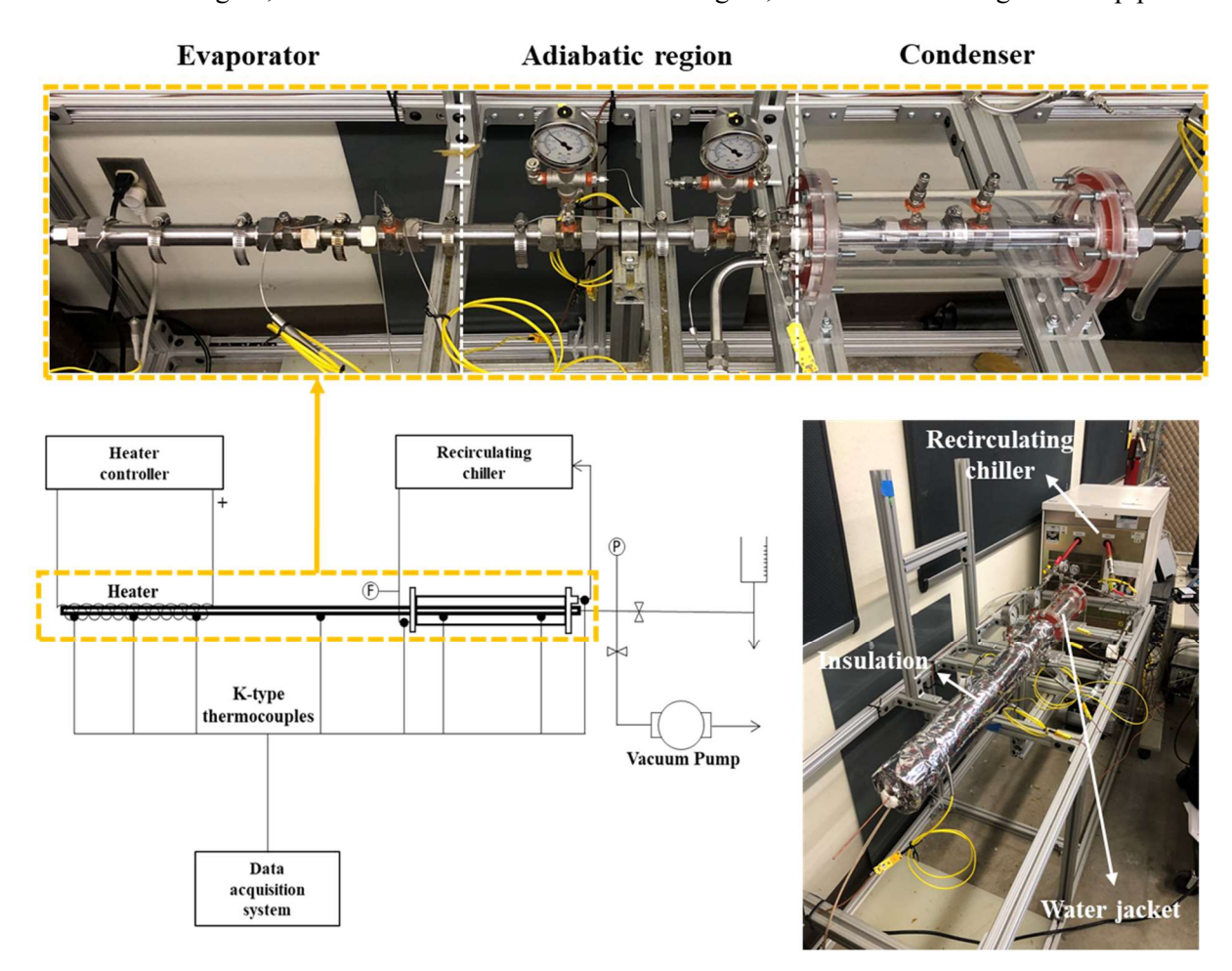


Figure 5. The schematic and the picture of the heat pipe experimental setup

2.2.2. Experimental Conditions

The heat pipe performance experiment was designed to evaluate the capillary limitation of the heat pipe, a key parameter that defines the heat removal capabilities of a heat pipe at a given temperature. Inside of the heat pipe, the liquid which condensates in the condenser is passively returned to the evaporator by the capillary force of the wick structure. The capillary limitation is the maximum power that the heat pipe can carry while keep returning the condensate by capillary force. Thus, the capillary limitation of a heat pipe can be calculated from Eq.4 which explains the amount of the power that the capillary force no longer overcome the pressure drop due to gravity, liquid flow, and vapor flow.

$$Q_{capillary} = \frac{2\sigma}{r_{e\!f\!f}} \frac{KA_{wick}h_{l\!v}\rho_l}{\mu_l L_{e\!f\!f}} = \frac{K}{r_{e\!f\!f}} \frac{2\sigma A_{wick}h_{l\!v}\rho_l}{\mu_l L_{e\!f\!f}}$$
 Eq.4 Here, $h_{l\!v}$ is the latent heat of the working fluid, and $L_{e\!f\!f}$ is the effective length of a heat pipe which can be

calculated from Eq.5.

$$L_{eff} = 0.5L_E + L_A + 0.5L_C$$
 Eq.5

where, L_E , L_A , and L_C presenting length of evaporator, adiabatic region, and condenser of the heat pipe, respectively. In Eq.4, the pressure drop due to the vapor flow is assumed to be negligibly small, and the heat pipe is in the horizontal position so that the gravitational pressure drop is also negligible.

Two boundary conditions are controlled in this study: the operating temperature and input power. Operating temperature is controlled from 50 °C to 80 °C by adjusting the temperature and flow rate of the coolant traveling through the water jacket. The power imposed to the evaporator section of the heat pipe is controlled and monitored using a transformer and power meter. The range of the heating power is set from 100 W to 400 W. The ranges of the boundary condition are selected considering the geometry of the heat pipe and the properties of the working fluid. This study focuses on the hydraulic parameters of the mesh structure, such as porosity, permeability, and effective pore radius. Since the capillary limitation is highly affected by those parameters, the expected range which the capillary limitation might occur is selected based on the calculation result of Eq.4.

2.2.3. Experimental Procedure

The experimental procedure to measure the heat transfer performance of the heat pipe was performed as follows: First, the targeted heating power is applied to the evaporator region. The heating power increases both surface temperature and operating temperature of the heat pipe. Here, the operating temperature of the heat pipe can be indicated by the temperature of the vapor in the vapor core which is the same with the surface temperature of the adiabatic section. The temperature and the flow rate of the coolant traveling in the water jacket is controlled to adjust the operating temperature of the heat pipe. For example, if the operating temperature exceeds a specified value, coolant with a lower temperature and higher mass flow rate is provided to the water jacket to reduce the internal pressure of the heat pipe. After both heating power and operating temperature reach to the targeted values, steady state is determined by checking the temporal variation of the surface temperature. During steady state, temperature and pressure are measured for 5 minutes. Then, the heat input is increased to the next level and the same procedure is repeated.

To determine the limiting operating conditions, an experiment is performed by increasing the power input while maintaining the operating temperature until the limiting condition is found. The point at which the operating limitation is reached is indicated by monitoring the surface temperature of the heat pipe. The temperature of the evaporator region starts to rise rapidly when the heat pipe meets the operating limit due to a loss of heat transfer caused by dry out. To prevent the failure of the experimental setup, the heating was shut down when the rapid increase of the temperature is observed, and the boundary condition is marked as an operating limitation point.

3. Result and Discussion

3.1. Wick Characterization Experimental Results

Results of the wick characterization experiments for 9 types of multi-layered screen meshes are shown in

Table 2. The porosities of each mesh, determined by the mesh saturation experiment, were used in Eq.3 to determine the permeability and effective pore radius. Figure 6 presents the result of the mean absolute percent deviation between time values of the data set and calculated time using Eq.3 for case #8. Deviations calculated from five pairs are summed up and presented in the left side of Figure 6. The plane of the deviation in the sample space of permeability and effective pore radius has a shape of a trough. From the side views of the plot shown in the middle and the right side of Figure 6, a point with the minimum deviation can be identified and its respective permeability and effective pore radius was selected as the true value. The composite wick case #8, for example, is determined to have a permeability of $0.635 \times 10^3 \mu m^2$ and a 0.169 mm effective pore radius.

Like in the case of the porosity measurement, the uncertainty of the measurements is quantified by repeating the same procedure and by checking the amount of the deviation. The experimental procedure starting from constructing the wick assembly with a single type of wick structure and fixed gap distance is repeated 27 times and the deviation of the permeability calculation is calculated. As a result, the data has $\pm 4.71\%$ of standard deviation when they are compared with averaged value.

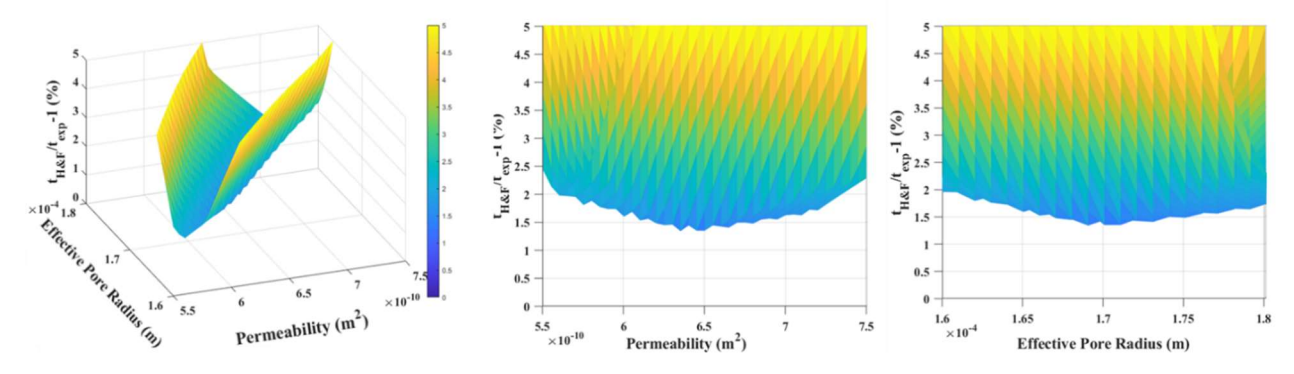


Figure 6. The result of the mean absolute percent deviation between time values of the data set and calculated time in a sample space of permeability and effective pore radius (left: 3D view, middle: permeability side view, right: effective pore radius side view).

Experimental results show that mesh case #2, which was built with 6 layers of the finest mesh (400-mesh), has the highest porosity, the lowest permeability, and the smallest pore radius. This is consistent with the geometric characteristics of the mesh. Among the three types of screen meshes used in this study, the 400-mesh has the highest porosity and the smallest pore size and the lowest permeability. On the other hand, mesh case #5 has the highest permeability.

From Eq.4, it can be recognized that the value of K / r_{eff} determines the capillary limitation of the heat pipe when the other geometric parameters and liquid properties are the same. In this study, therefore, the value of K / r_{eff} is checked as a parameter of interest for the wick performance.

From

Table 2, it can be noticed that the composite mesh case #5 is expected to provide the highest capillary limitation when it is installed inside the heat pipe. Because the geometry of the composite wick structure is not homogeneous, the phenomena that occur inside of it are complex and highly unpredictable. This results in a lack of the analytical model to optimize the design of the wick structure. In this study, therefore, several samples of wick structures were built, and their hydraulic parameters were measured by relatively simple experimental methods. As will be shown by the results from the heat pipe performance experiment, these measured parameters can be effectively used to predict the operating limitations of a heat pipe.

Table 2. Result of the wick characterization experiment for various types of multi-layered screen meshes.

Case #	Total number of layers	Mesh composition			Measurement result			
		100- mesh (inside layer)	400- mesh (middle layer)	60-mesh (outside layer)	Porosity (ε [-])	Permeability (K [μm²])	Effective Pore Radius $(r_{eff}[mm])$	$rac{K}{r_{eff}} \ [\mu m]$
1	6	6	0	0	0.642	0.815×10^3	0.266	3.064×10^3
2		0	6	0	0.767	0.825×10^3	0.232	3.556×10^3
3		0	0	6	0.626	0.745×10^3	0.419	1.778×10^3
4		2	2	2	0.634	0.985×10^3	0.252	3.909×10^3
5		1	3	2	0.653	1.435×10^3	0.213	6.737×10^3
6		2	3	1	0.667	1.205×10^3	0.264	4.564×10^{3}
7		2	1	3	0.637	0.300×10^3	0.188	1.596×10^{3}
8		3	2	1	0.671	0.635×10^3	0.169	3.757×10^3
9		3	1	2	0.682	1.080×10^3	0.284	3.803×10^3

3.2. Results of the gap effect

The investigation on the effect of the gap between the wick and the wall was conducted by measuring performance of a wick structure with different gap distances. The mesh case #5 was selected as a testing sample since it showed the best performance among different combinations of multiple screen meshes.

From Eq.3, multiple pairs of experimental data for the mass (m_{exp}) and the time (t_{exp}) are required to find the two unknown variables, permeability (K) and the effective pore radius (t_{exp}) . If only a single pair of the data is used, on the other hand, one could not obtain the solution of the equation but can still check the relationship between the permeability and the effective pore radius. Figure 77 shows the line on the sample

space of permeability and the effective pore radius which results in a solution to Eq.3. These lines were determined using a single pair of the data at measured at t = 5s. The lines which indicate the relationship between the two parameters show the performance of the mesh. Based on the discussion above, K / r_{eff} is an important parameter of the mesh when the capillary limitation of the heat pipe is considered. In the same perspective, the slope of the lines in Figure 77 might be an indicator of the wick performance. For example, wicks with 0.7 mm and 1.2 mm of gap distance from the wall show the smallest slope in the plot which means the largest K / r_{eff} value. On the other hand, the bare mesh without any wall shows the smallest K / r_{eff} value, inferring the lowest performance.

As mentioned above, a unique solution of the permeability and effective pore radius can be found when multiple pairs of data are used. In the ideal case, a single line on the sample space will be created for each pair of mass and time data, and lines will be crossed at a point, which is a unique solution. Thus, even though the lines in Figure 7 are calculated using only a single pair of data, the actual permeability and effective pore radius values of the mesh with various gap distances lay on the line. In this point of view, a lower effective pore radius and a higher permeability could be expected for the mesh with $0.7 \sim 1.2$ mm of gap distance compared to the bare mesh. This approach might be meaningful because obtaining a solution for Eq.3 is achieved by an iterative method and bringing more pairs of data into the calculation increases the computational cost linearly. The result from only one pair of data could provide valuable intuition about the performance of the wick structure while reducing the time required to determine a more exact solution. This may be especially useful for a study is focused on the comparison of multiple wicks where computational costs would quickly increase.

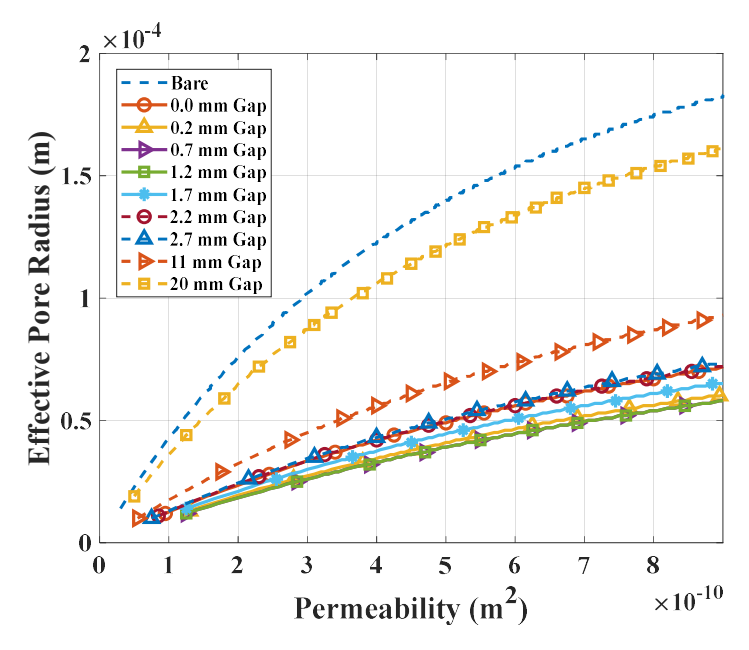


Figure 7. The relationship between permeability and effective pore radius of the wick structure with varying gap distance.

Figure 8 shows the result of the calculations with 5 pairs of mass and time data collected from the experiment. Unlike the results with a single pair of data introduced above, a point which has the minimum mean absolute percent deviation can be found in the space of permeability and effective pore radius. To investigate the effect of the gap distance on the two parameters, the results are plotted against the gap distance. In the plot on the left side of the figure, the permeability increases as the gap becomes wider, with

a peak at a gap distance of 1.2 mm. As the gap increases more, the permeability can be seen to become smaller and converge to the bare mesh case. On the other hand, the effective pore radius is shown to behave inversely of the pore radius in the right figure. The effective pore radius become smaller as the gap increases with a peak at 0.7 mm of distance.

An interesting point can be found from the results of the 0 mm gap case. Considering that a wick with higher permeability and smaller effective pore radius has better performance, the mesh with a 0 mm gap can be noticed to have better performance than the bare mesh case. This is because the geometry of the screen mesh creates micro channels even though it is attached to the wall. These channels provide extra capillary pressure and flow paths for the fluid. The large difference with bare mesh emphasizes the necessity of further studies on the impact of wall effects on heat pipe performance.

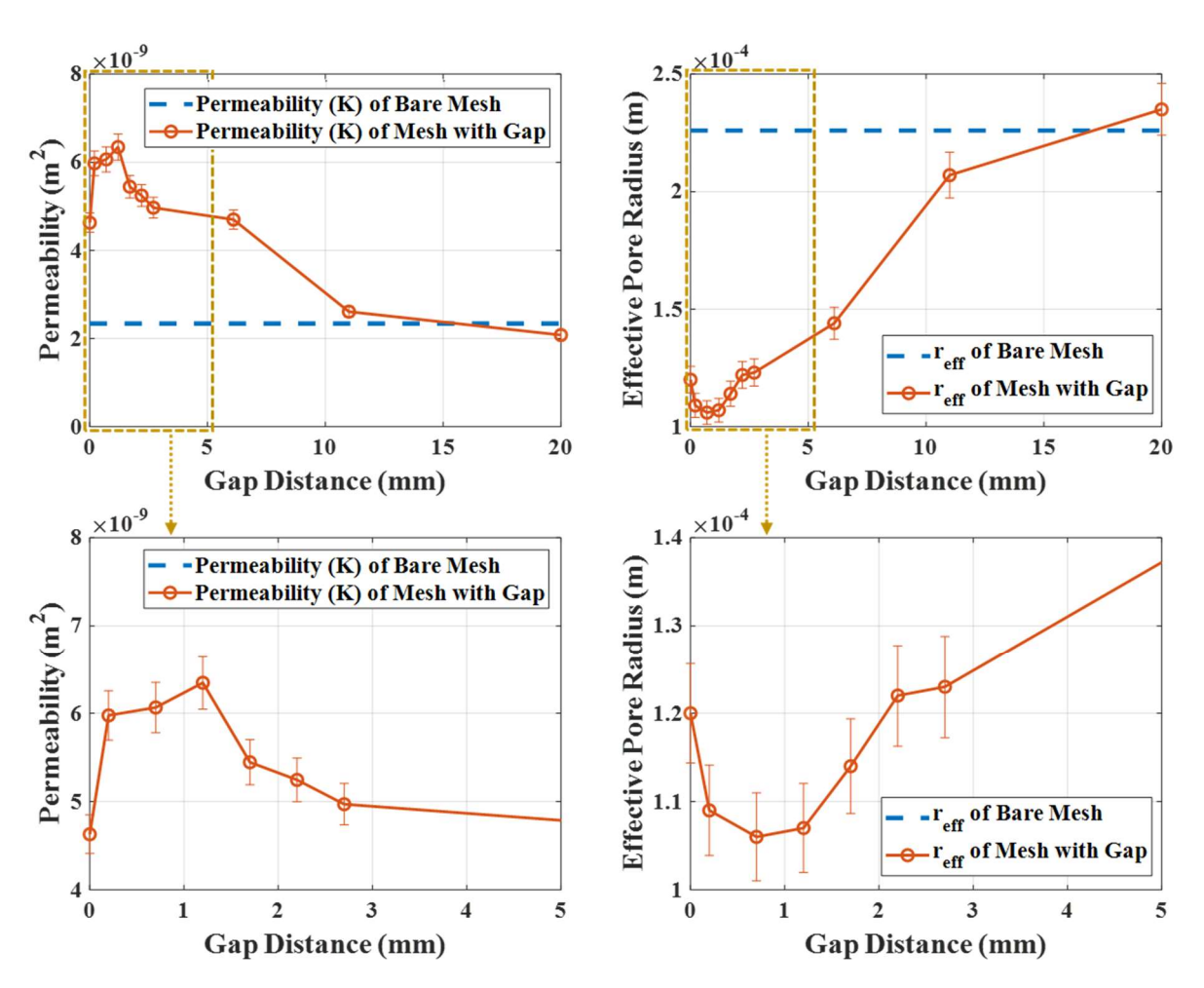


Figure 8. The result of permeability (left) and effective pore radius (right) measurement of the wick structure with varying gap distance.

The result of the $_{K/r_{eff}}$ calculation is plotted against gap distance in Figure 9. An increasing trend from 0 mm to 1.2 mm, and a decreasing trend from 1.2mm to 20 mm with convergence to bare mesh results were observed. The enhancement of the performance gained by the gap can be explained in two ways. First,

additional capillary pressure is created by the gap. Since the space between the inner surface of the tube and the outer surface of the mesh structure consists of a narrow cylindrical channel, extra capillary pressure is generated and reduces the effective pore radius from an axis-symmetric form of the Laplace-Young equation which is as follows:

$$\Delta P_{capillary} = \frac{2\sigma\cos\theta}{r} = \frac{2\sigma}{r_{eff}}$$
 Eq.6

Second, the channel created by the gap provides an additional flow path for the working fluid which reduces the pressure drop. The reduced pressure drop is reflected in the increased permeability of the wick structure.

From the explanation above, it can be seen that the two effects become competing factors to one another when they are explained using gap distance. The additional capillary pressure from the gap is maximized when the smallest gap distance is introduced. This can be easily recognized from Eq.6. On the other hand, the pressure drop due to the shear stress of the channel is reduced when the diameter of the channel, the gap distance in this study, is increased. Due to this trade-off of two benefits, there must be an optimal gap distance to produce the largest benefit to heat pipe performance. In this study, the optimal gap distance which gives the best wick performance was experimentally found to be 1.2 mm. This value only includes effects on hydraulic characteristics of the wick structure, not on thermal characteristics of the wick. The gap might increase the thermal resistance in the radial direction of the heat pipe when a working fluid with low thermal conductivity is used. This impact may be less significant in real scenarios as annular type multi-layered composite screen mesh heat pipes are mainly used with high conductivity liquid metals as the working fluid. The experimental data provided in this study which relates to the optimal gap distance may be of value as it has not been addressed in current literature.

Its claimed ideal gap spacing, however, is purely dependent on the capillary limit. Other gap spacing may be more acceptable depending on the operating temperature range and its associated operating limitation. Other significant performance constraints could be functions of fluid characteristics as well as geometrical parameters. Furthermore, there are a few other things that can influence the size of an optimal annular gap during the operation of the heat pipe. The highest diametral gap bound is often constrained by vertical priming around the heat pipe circumference for horizontal operation in a gravitational field. The working fluid parameters, such as density and surface tension, play an important role in the priming of the gap. The priming condition could potentially influence the optimal gap size and needs to be investigated through further studies.

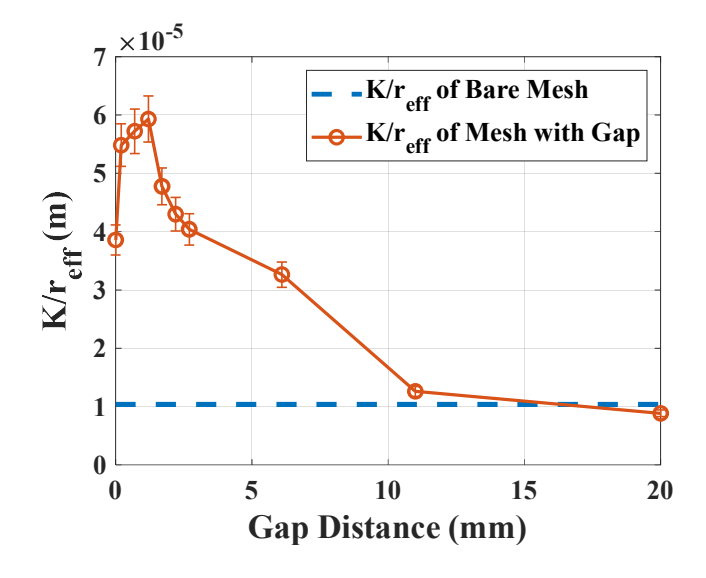


Figure 9. The result of K/r_{eff} measurement of the wick structure with varying gap distance.

3.3. Heat Pipe Performance Experimental Results

The results presented above are based on the experiments with thoroughly controlled local parameters. In practice, however, a single annular heat pipe wick can have a wide range of gap topologies, ranging from concentric annular to crescent annular, depending on the position. Furthermore, heat pipe wicks rarely have a single pore radius; rather, the pore radius follows a log-normal distribution. It can be questionable whether the results made from the result above might be also useful for an actual annular wick type heat pipe which its characteristics are presented with overall averaged value instead of a local value. Thus, sets of experiments were performed on the heat pipe with concentric annular type wick structure to check its capillary limit can be predicted by the values measured in this study.

Figure 10 presents the results of the experiment. Points marked as circles indicate when the heat pipe was operating in normal conditions. The boundary conditions where heat pipe encountered capillary limitation, determined by a rapid increase in surface temperature, are marked with a cross. With some boundary conditions, temperature fluctuations occurred for several minutes with no rapid temperature increase. These points, marked with triangles, are considered a boundary between the normal operation heat pipe failure.

The capillary limitation of the bare mesh was calculated from Eq.4 using the $_{K/r_{eff}}$ ratio determined by the mesh characterization experiment results. The calculated value of the bare mesh is used as a standard value to calculate the capillary limitation of the heat pipe with an annular type wick structure. The main idea here is that the capillary limitation calculated from Eq.4 is assumed to present the limitation of the heat pipe without a gap between the wall and mesh. Based on this, a multiplying factor (G) is introduced. The factor was calculated simply by dividing $_{K/r_{eff}}$ values of the wick structure with different gap distances which is presented in Figure 9 by a $_{K/r_{eff}}$ value of the wick with 0 mm gap distance. The results are shown in Table 3. By introducing the multiplying factor, the capillary limitation of the heat pipe with an annular type wick structure can be calculated using the following equation.

$$Q_{capillary.gap} = G \cdot Q_{capillary} = G \frac{2\sigma}{r_{eff}} \frac{KA_{wick}h_{lv}\rho_{l}}{\mu_{l}L_{eff}}$$
 Eq.7

Based on the gap distance of 0.95 mm, a value was 1.51 was used for the G value of the current heat pipe. As shown in Figure 10, this prediction is in strong agreement with the experimental results. As expected, heat pipe normally operates above the predicted power by traditional correlation without the consideration of the gap effect. Based on the result, the correlation suggested in this study can be used to predict the capillary limitation of the heat pipe with annular wick structure instead of the one suggested for the heat pipe without any gap between the wick structure and the wall.

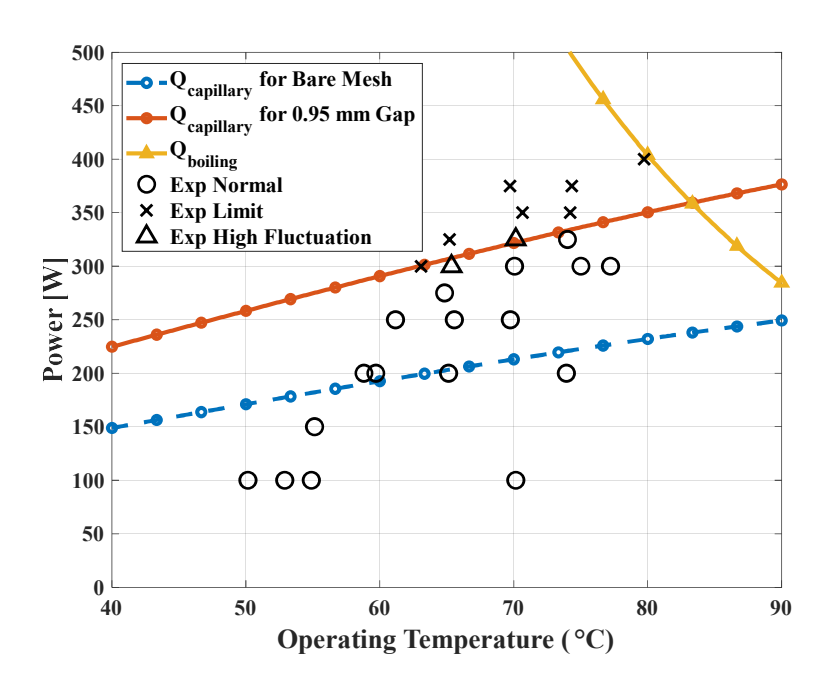


Figure 10. The result of heat pipe operating limitation experiment.

Table 3. Gap multiplying factor for capillary limitation.

Gap Distance	G
[mm]	[-]
0	1.00
0.2	1.42
0.7	1.48
1.2	1.54
1.7	1.24
2.2	1.11
2.7	1.05

4. Conclusion

In this study, an experimental investigation was conducted on the hydraulic characteristics of annular type wick structures for heat pipes. An experimental facility was developed to measure porosity, permeability, and effective pore radius of wick structures in vacuum condition. Also, a heat pipe with an annular type wick structure was built and its capillary limitation was determined.

Through the experimental investigation, the following results were found.

• Nine different types of multi-layered (6 layers in total) composite screen meshes were characterized. Based on the measurement results, a wick structure composed of one layer of a 100x100 mesh, three layers of a 400x400 mesh, and two layers of a 60x60 mesh is determined to have the best performance.

- The gap effect on the hydraulic characteristics of annular type wick structures is investigated. The measured permeability and effective pore radius of a wick with different gap distances showed that there is an optimal point in gap distance which was found to be 1.2 mm.
- The effect of the gap to performance of the heat pipe is tested using a heat pipe with an annular type wick structure. A multiplying factor to account for the enhanced performance of the wick provided by the gap is suggested. The calculated result showed good agreement with the experimental results.

Phenomena occurring inside of heat pipes is highly complicated and is not yet fully understood. While there are many models suggested by previous studies, models for heat pipes with annular type wick structures are limited to non-existent. This work provides insights into optimized design parameters and improved modeling methods, essential for the construction of systems utilized annular heat pipes. This study also lays the groundwork for additional works with similar approaches and extended experiments to provide further understanding of phenomena occurring within annular, composite mesh wick heat pipes, as well as data for the validation of new models.

ACKNOWLEDGMENTS

The authors gratefully acknowledge the partial financial support from the Nuclear Energy University Program (NEUP) of the Department of Energy (DOE).